Determination of the water vapor continuum absorption by THz-TDS and Molecular Response Theory

Yihong Yang, Mahboubeh Mandehgar, and D. Grischkowsky*

School of Electrical and Computer Engineering, Oklahoma State University, Stillwater, Oklahoma 74078, USA
*daniel.grischkowsky@okstate.edu

Abstract: Determination of the water vapor continuum absorption from 0.35 to 1 THz is reported. The THz pulses propagate though a 137 m long humidity-controlled chamber and are measured by THz time-domain spectroscopy (THz-TDS). The average relative humidity along the entire THz path is precisely obtained by measuring the difference between transit times of the sample and reference THz pulses to an accuracy of 0.1 ps. Using the measured total absorption and the calculated resonance line absorption with the Molecular Response Theory lineshape, based on physical principles and measurements, an accurate continuum absorption is obtained within four THz absorption windows, that agrees well with the empirical theory. The absorption is significantly smaller than that obtained using the van Vleck-Weisskopf lineshape with a 750 GHz cut-off.

OCIS codes: (010.1030) Absorption; (010.1320) Atmospheric transmittance; (300.6495) Spectroscopy, terahertz.

References and links

1. S. Paine, R. Blundell, D. Papa, J. Barrett, and S. Radford, "A Fourier transform spectrometer for measurement of atmospheric transmission at submillimeter wavelengths," Publ. Astron. Soc. Pac. **112**(767), 108–118 (2000).
2. E. Cianca, T. Rossi, A. Yahalom, Y. Pinhasi, J. Farserotu, and C. Sacchi, "EHF for satellite communications: the new broadband frontier," Proc. IEEE **99**(11), 1858–1881 (2011).
3. J. S. Melinger, Y. Yang, M. Mandehgar, and D. Grischkowsky, "THz detection of small molecule vapors in the atmospheric transmission windows," Opt. Express **20**(6), 6788–6807 (2012).
4. Y. Yang, M. Mandehgar, and D. Grischkowsky, "Understanding THz pulse transmission in the atmosphere," IEEE Trans. THz Sci. Technol. **2**(4), 406–415 (2012).
5. H. J. Liebe, "The atmospheric water vapor continuum below 300 GHz," Int. J. Infrared Millim. Waves **5**(2), 207–227 (1984).
6. L. S. Rothman, I. E. Gordon, A. Barbe, D. C. Benner, P. F. Bernath, M. Birk, V. Boudon, L. R. Brown, A. Campargue, J.-P. Champion, K. Chance, L. H. Coudert, V. Dana, V. M. Devi, S. Fally, J.-M. Flaud, R. R. Gamache, A. Goldman, D. Jacquemart, I. Kleiner, N. Lacome, W. J. Lafferty, J.-Y. Mandin, S. T. Massie, S. N. Mikhailenko, C. E. Miller, N. Moazzen-Ahmadi, O. V. Naumenko, A. V. Nikitin, J. Orphal, V. I. Perevalov, A. Perrin, A. Predoi-Cross, C. P. Rinsland, M. Rotger, M. Šimečková, M. A. H. Smith, K. Sung, S. A. Tashkun, J. Tennyson, R. A. Toth, A. C. Vandaele, and J. Vander Auwera, "The HITRAN 2008 molecular spectroscopic database," J. Quantum Spectrosc. Radiat. Transfer **110**(9–10), 533–572 (2009).
7. H. M. Pickett, R. L. Poynter, E. A. Cohen, M. L. Delitsky, J. C. Pearson, and H. S. P. Muller, "Sub-millimeter, millimeter, and microwave spectral line catalog," J. Quantum Spectrosc. Radiat. Transfer **60**(5), 883–890 (1998); Access to specific catalog entries may be found at http://spec.jpl.nasa.gov/.
8. R. J. Hill, "Water vapor-absorption lineshape comparison using the 22-GHz line: the Van Vleck-Weisskopf shape affirmed," Radio Sci. **21**(3), 447–451 (1986).
9. M. A. Koshelev, E. A. Serov, V. V. Parshin, and M. Yu. Tretyakov, "Millimeter wave continuum absorption in moist nitrogen at temperature 261-328K," J. Quantum Spectrosc. Radiat. Transfer **112**(17), 2704–2712 (2011).
10. M. Y. Tretyakov, A. F. Krupnov, M. A. Koshelev, D. S. Makarov, E. A. Serov, and V. V. Parshin, "Resonator spectrometer for precise broadband investigations of atmospheric absorption in discrete lines and water vapor related continuum in millimeter wave range," Rev. Sci. Instrum. **80**(9), 093106 (2009).
11. T. Kuhn, A. Bauer, M. Godon, S. Buhler, and K. Kunzi, "Water vapor continuum: absorption measurements at 350GHz and model calculations," J. Quantum Spectrosc. Radiat. Transfer **74**(5), 545–562 (2002).

#201718 - $15.00 USD Received 21 Nov 2013; revised 10 Feb 2014; accepted 11 Feb 2014; published 19 Feb 2014

12. V. B. Podobedov, D. F. Plusquellic, K. E. Siegrist, G. T. Fraser, Q. Ma, and R. H. Tipping, "New measurements of the water vapor continuum in the region from 0.3 to 2.7 THz," J. Quantum Spectrosc. Radiat. Transfer **109**(3), 458–467 (2008).
13. D. M. Slocum, E. J. Slingerland, R. H. Giles, and T. M. Goyette, "Atmospheric absorption of terahertz radiation and water vapor continuum effects," J. Quantum Spectrosc. Radiat. Transfer **127**, 49–63 (2013).
14. P. W. Rosenkranz, "Water vapor microwave continuum absorption: a comparison of measurements and models," Radio Sci. **33**(4), 919–928 (1998).
15. J. H. Van Vleck and V. F. Weisskopf, "On the shape of collision-broadened lines," Rev. Mod. Phys. **17**(2–3), 227–236 (1945).
16. C. H. Townes and A. L. Schawlow, *Microwave Spectroscopy* (Dover, 1975).
17. Y. Yang, M. Mandehgar, and D. Grischkowsky, "Broad-band THz pulse transmission through the atmosphere," IEEE Trans. THz Sci. Technol. **1**(1), 264–273 (2011).
18. D. Grischkowsky, S. Keiding, M. van Exter, and C. Fattinger, "Far-infrared time-domain spectroscopy with terahertz beams of dielectrics and semiconductors," J. Opt. Soc. Am. B **7**(10), 2006–2015 (1990).
19. Y. Yang, A. Shutler, and D. Grischkowsky, "Measurement of the transmission of the atmosphere from 0.2 to 2 THz," Opt. Express **19**(9), 8830–8838 (2011).
20. Y. Yang, M. Mandehgar, and D. Grischkowsky, "Time domain measurement of the THz refractivity of water vapor," Opt. Express **20**(24), 26208–26218 (2012).
21. H. Harde, N. Katzenellenbogen, and D. Grischkowsky, "Line-shape transition of collision broadened lines," Phys. Rev. Lett. **74**(8), 1307–1310 (1995).
22. H. Harde, R. A. Cheville, and D. Grischkowsky, "Terahertz studies of collision broadened rotational lines," J. Phys. Chem. A **101**(20), 3646–3660 (1997).
23. D. Grischkowsky, Y. Yang, and M. Mandehgar, "Zero-frequency refractivity of water vapor, comparison of Debye and van-Vleck Weisskopf theory," Opt. Express **21**(16), 18899–18908 (2013).
24. M. Mandehgar, Y. Yang, and D. Grischkowsky, "Atmosphere characterization for simulation of the two optimal wireless terahertz digital communication links," Opt. Lett. **38**(17), 3437–3440 (2013).
25. D. E. Burch and D. A. Gryvnak, "Continuum absorption by water vapor in the infrared and millimeter regions," in *Atmospheric Water Vapor*, A. Deepak, ed. (Academic, 1980), pp. 47–76.
26. J. H. van Vleck, "The absorption of microwaves by oxygen," Phys. Rev. **71**(7), 413–424 (1947).

1. Introduction

Water vapor plays the dominant role in the propagation of mm and THz electromagnetic waves in the atmosphere, since it has several thousand rotational absorption lines from the mm wave range through the terahertz region up to 5 THz. Also, oxygen gas has a cluster of approximately 25 overlapping lines at 60 GHz and a single line at 120 GHz. The atmospheric mm and THz windows, which are located between the strong resonant lines from 10 GHz up to approximately 2 THz allow for variable range transmission of THz pulses depending on the window. However, an additional continuum absorption exists within the transparent THz windows, which cannot be explained by the far-wing absorption of the resonant lines. The measurements and understanding of the continuum absorption are important in many aspects of physics of the atmosphere, such as ground and satellite-based radio astronomy [1], communication links [2], and remote spectroscopic applications [3].

The poorly understood continuum absorption is determined empirically and is defined as the difference between the measured total absorption and the absorption of the resonant lines [4]. The latter is usually calculated as the sum of all of the resonant lines based on a lineshape function with the corresponding line intensity and linewidth of individual lines, taken from a spectroscopic database, such as the Millimeter wave Propagation Model (MPM) [5], HITRAN [6] and JPL [7]. The determined continuum absorption depends strongly on the lineshape function, number of lines, line intensities and linewidth chosen for the line-by-line summation method. It has been shown that the van Vleck-Weisskopf (vV-W) lineshape fits the resonant lines near their centers more accurately than the full Lorentz (FL) and Gross lineshapes [8]. Since then, in most of the literature the vV-W lineshape has used to obtain the continuum absorption within the Millimeter wave [5,9,10] and THz regions [11–13] under various humidity and temperature conditions. Clearly, only the resonance absorption with a strictly defined lineshape function can lead to reliable values of the continuum absorption.

However, two types of vV-W lineshape functions are found in the literature, regarding determinations of the continuum absorption: those with a linear ν/ν_j pre-factor [11–13], and

#201718 - $15.00 USD Received 21 Nov 2013; revised 10 Feb 2014; accepted 11 Feb 2014; published 19 Feb 2014

those with a quadratic $(v/v_j)^2$ pre-factor [5,8–10,14]. In this paper, we will show the quadratic pre-factor agrees with the original vV-W paper [15] and with Townes and Schawlow [16].

Many recent works have obtained the relative continuum absorption by subtracting the resonance absorption based on the quadratic pre-factor vV-W lineshape function, but with a cutoff frequency of 750 GHz from the line center. We will show by using molecular response theory, that this cut-off is too severe and thereby gives a lower value for the resonant line absorption and a consequent higher value for the continuum absorption.

Most of the experimental studies of the water vapor continuum absorption in the mm wave and THz region have used a Fabry-Perot interferometer (FP) or a Fourier transform spectrometer (FTS) equipped with a multi-pass cell [11,12]. An experimental problem for these approaches is significant absorption from an adsorbed layer of water on the reflectors surfaces, which increases with humidity. A new approach based on the variation of the spectrometer optical path-length was proposed to solve this problem [9,10]. However, the mismatch of the distribution of electrical field, coupling loss and the water adsorption on the resonator elements could cause systematic error. The most recent work utilizes a Fourier Transform Infrared (FTIR) spectrometer equipped with a long-path cavity of 1-6 m length [13]. Our THz-TDS long-path setup minimizes the systematic uncertainty from adsorption on chamber elements, having less than 0.4% double pass amplitude loss on 100 nm thick water layers on two mirrors with 45 degree incident angle and essentially no loss with normal incidence on the other eight mirrors [17].

The techniques of FTIR and THz-TDS have been compared in previous work [3]. Although both of them have similar frequency resolution and comparable spectral S/N ratio. However, the gated and coherent detection of THz-TDS [18,19] can avoid the continuous thermal noise background, thereby giving a much higher sensitivity at room temperature than the incoherent liquid helium cooled bolometers of FTS. Another powerful advantage of THz-TDS is that the electric field pulse is measured, compared to FTS, which typically measures the transmitted THz power.

In this paper, we measured the relative total water vapor absorption, using a 137 m round-trip humidity controlled sample chamber within the 170 m long-path THz-TDS system, that measures the water density from the transit time of the THz pulses [20]. For our analysis, we use the fundamental molecular response theory (MRT) [21,22], based on physical principles and measurements, to obtain the resonant line absorption.

MRT resonant absorption consists of a frequency dependent fractional sum of the vV-W absorption and the full Lorentz (FL) absorption, $\alpha^{MRT}(\nu) = S(\nu)\,\alpha^{vV\text{-}W}(\nu) + [1- S(\nu)]\,\alpha^{FL}(\nu)$, where $S(\nu)$ is the weighting factor, determined by the molecular response time $\tau_c = 0.2$ ps [21,22]. Consequently, the MRT resonant absorption is always between the vV-W and FL values of absorption, which provides fundamental limits to the resonant line absorption.

We will show that for the atmosphere at the relatively normal conditions of 20 ^{o} C and RH 36.2% (7.0 g/m^3), the continuum absorption below 1 THz is easily determined in all of our 4 THz windows of transparency. For the highest frequency window at 850 GHz the total measured absorption is 56 dB/km; the calculated MRT absorption is 40 dB/km, thereby giving the continuum absorption of 16 dB/km. In comparison, under these same conditions, the approximate vV-Wc absorption is calculated to be only 33 dB/km, thereby giving the increased continuum absorption of 23 dB/km.

2. Theory

2.1 van Vleck-Weisskopf (vV-W) lineshape

In the JPL database the absorption coefficient $\alpha_j(v)$ of water vapor resonant line can be written as the product of a line intensity I_j with units of (nm^2 MHz) and a lineshape function $f(v, v_j)$ [4,7]: where N_{H2O} is the number density of water vapor in molecules / (cm·nm^2), and v_j is the resonant line center frequency in MHz.

#201718 - $15.00 USD Received 21 Nov 2013; revised 10 Feb 2014; accepted 11 Feb 2014; published 19 Feb 2014

$$\alpha_j(v) = N_{H2O} \cdot I_j(v) \cdot f(v, v_j). \tag{1}$$

For both the JPL and the HITRAN databases, the total absorption coefficient is the sum of all the individual water vapor absorption lines, $\alpha = \sum_j \alpha_j$. The two types of vV-W lineshape equations are given in different works as:

$$f_1(v, v_j) = \frac{1}{\pi}\left(\frac{v}{v_j}\right)^2 \cdot \left(\frac{\Delta v_j}{(v - v_j)^2 + \Delta v_j^2} + \frac{\Delta v_j}{(v + v_j)^2 + \Delta v_j^2}\right). \tag{2}$$

$$f_2(v, v_j) = \frac{1}{\pi}\left(\frac{v}{v_j}\right) \cdot \left(\frac{\Delta v_j}{(v - v_j)^2 + \Delta v_j^2} + \frac{\Delta v_j}{(v + v_j)^2 + \Delta v_j^2}\right). \tag{3}$$

where Δv_j is the line half-width at half-maximum (HWHM), and v_j is line center frequency. The only difference between these two functions is that Eq. (2) has a quadratic, and Eq. (3) has a linear v/v_j pre-factor. The amplitude transmissions based on these two types of v-VW line shapes are shown in Appendix A. The quadratic pre-factor vV-W lineshape function is shown in Appendix A to be required for the JPL database, based on the direct conversion of the absorption expression in the original vV-W paper [15].

The HITRAN equation was used in the calculation and analysis in the following sections, because HITRAN gives the line broadening coefficients, which are used to calculate the corresponding line half-width for all of the individual water vapor lines. All of the conclusions apply to both the JPL and the HITRAN databases, which yield identical results.

2.2 vV-W lineshape functions with cut-off frequency (vV-Wc)

The vV-W lineshape has an unphysical constant value in far-wings [8], which will lead to a divergence of the lineshape integral over frequency. A cutoff method for the far-wings was introduced to solve this problem [14]. The choice of 750 GHz for the cutoff frequency has been customary in many studies [9,11,14],and is related to an assumed 1 ps "duration" of the molecular collisions. This model is discussed in Appendix B. Using the new molecular response theory (MRT) [21,22], we will show in Fig. 1, that the cut-off model over-states the continuum absorption.

2.3 Connection of the vV-W and FL lineshapes by molecular response theory (MRT)

Previous THz-TDS measurements of the absorption of the far-wings of the resonant lines of methyl halide vapors out to more than 200 line-widths from resonance, and corresponding to as much as 5 times the resonant frequency, observed a smooth transition from the vV-W lineshape to the full Lorentz lineshape (FL) with increasing frequency [21,22]. These observations were well fit by a new molecular response theory (MRT), which includes the molecular orientation time τ_c during a collision [21,22]. For these measurements, the response time was $\tau_c = 0.2$ ps [21,22].

For the molecular response theory the absorption lineshape function is given by

$$\alpha_j^{MRT}(v) = S(v)\,\alpha_j^{vV-W}(v) + (1 - S(v))\,\alpha_j^{L}(v). \tag{4}$$

for which $\alpha_j^{vV-W}(v)$ is the lineshape function of the vV-W theory, in Eq. (2), and $\alpha_j^{L}(v)$ is the FL lineshape function, and $S(v)$ is the MRT weighting function controlling the transition from the vV-W lineshape at low frequencies to the FL lineshape at higher frequencies. S(v) is given simply by,

#201718 - $15.00 USD Received 21 Nov 2013; revised 10 Feb 2014; accepted 11 Feb 2014; published 19 Feb 2014

$$S(\nu) = 1\Big/\left[1+(2\pi\nu\tau_c)^2\right]. \tag{5}$$

where τ_c is the collision parameter. S(ν) monotonically changes from one to zero as the frequency increases, and S(ν) = 0.5 for $\nu_{1/2} = 1/(2\pi\tau_c)$ = 796 GHz for τ_c = 0.2 ps. Consequently, for $2\pi\nu\tau_c \ll 1$, $\alpha_j^{MRT}(\nu) \approx \alpha_j^{vV-W}(\nu)$, and for $2\pi\nu\tau_c \gg 1$, $\alpha_j^{MRT}(\nu) \approx \alpha_j^{L}(\nu)$. τ_c is considered to be a measure of the orientation time of molecules during a collision and is expected to be much faster than the duration of a collision. Consistent with the notation of Eq. (2) for the vV-W lineshape, the corresponding full Lorentz (FL) lineshape is given by [8,15,21,22].

$$f_L(\nu,\nu_j) = \frac{1}{\pi}\left(\frac{\nu}{\nu_j}\right)\cdot\left(\frac{\Delta\nu_j}{(\nu-\nu_j)^2+\Delta\nu_j^2} - \frac{\Delta\nu_j}{(\nu+\nu_j)^2+\Delta\nu_j^2}\right). \tag{6}$$

Note that the FL lineshape has the linear pre-factor and the negative sign for the second term in the brackets. The comparison of the vV-W, FL, MRT and vV-Wc absorption lineshapes on the low and high-frequency wings, of a single resonance line at 1.0 THz and with a peak value of unity is shown in Fig. 1. Surprisingly, because of the linear pre-factor, the FL line is higher than the vV-W line on the low-frequency side, while on the high-frequency side, it is significantly lower as expected [21,22]. It is important to note that the MRT line, as defined in Eq. (4), will always be between the FL and the vV-W lines. This feature has only the linewidths as a parameter, which are calculated by HITRAN. The value of the MRT line located between the vV-W and FL lines is determined by τ_c = 0.2 ps [21,22].

As shown in Fig. 1, the MRT value of the resonant line absorption is between the vV-W and the FL lines. This is not the case for the much lower vV-Wc line, which significantly understates the resonant absorption, and thereby overstates the continuum absorption.

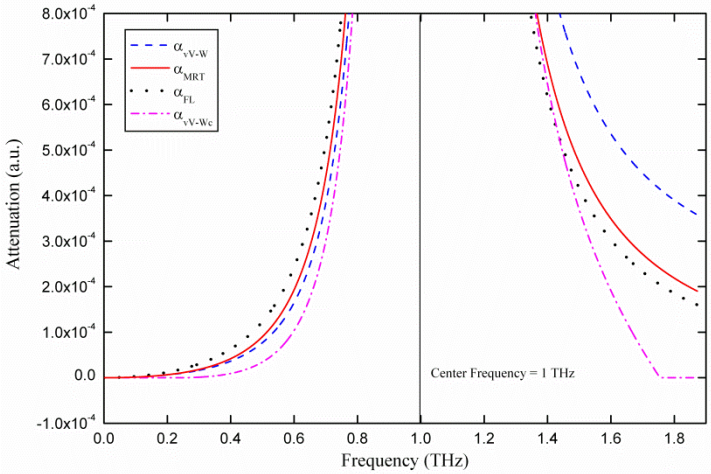

Fig. 1. Absorption line comparison for a single resonance line normalized to unity with center frequency at 1.0 THz. vV-W (dashed line), FL (dotted line), MRT (red line between vV-W and FL lines), and the Eqs. (2), (24), (25) vV-Wc (dash-dot line) showing the abrupt cut-off at 1.75 THz (750 GHz from line center). All lineshapes have (HWHM) linewidth of 3.15 GHz. For MRT, τ_c = 0.2 ps.

2.4. Empirical continuum absorption function

The experimentally verified [5,9,14] empirical equation of the continuum absorption α_c has two components: one part is proportional to the square of the water vapor partial pressure P_W; the other part is proportional to the product of P_W and the total of the foreign gas partial

#201718 - $15.00 USD Received 21 Nov 2013; revised 10 Feb 2014; accepted 11 Feb 2014; published 19 Feb 2014

pressures in the atmosphere P_A . This dependence is shown in Eq. (7) [5,9,14], and is in good agreement with high water vapor pressure and high temperatures experiments over a wide range [6,9,14].

$$\alpha_c(v,T) = v^2 \cdot \left(C_W^0 \cdot \theta^{n_s+3} \cdot P_W^2 + C_A^0 \cdot \theta^{n_f+3} \cdot P_A \cdot P_W \right). \quad (7)$$

In Eq. (7), C_W^0 and C_A^0 are the self and foreign continuum parameters at 300 K, in units of dB/km/(hPa GHz)^2, respectively. θ is the temperature factor, 300/T, n_s and n_f are their temperature exponents, and v is frequency in GHz. In this paper, we use $C_W = C_W^0 \cdot \theta^{n_s+3}$ and $C_A = C_A^0 \cdot \theta^{n_f+3}$ as the fitting parameters for all of the curves, obtained at 294 K. The atmospheric pressure P_A = 1004 hPa, equivalent to the density ρ_A = 1193 g/m^3, can be considered constant, since the variable water vapor partial pressure P_W is only of the order of 1% of P_A . The water vapor density ρ_W in g/m^3 can be obtained from P_W in hPa by multiplying by the factor of 0.752, similarly for air by 1.19. If we replace the pressure-related parameters C_W and C_A by the equivalent density-related parameters $C_W^* = (1/0.752)^2 C_W$ and $C_A^* = \left[1/(0.752 \times 1.19)\right] C_A$ respectively, Eq. (7) can then be rewritten as:

$$\alpha_c(v, 294K) = v^2 \left[C_W^* \cdot \rho_W^2 + C_A^* \cdot \rho_A \cdot \rho_W \right]. \quad (8)$$

In this work, instead of measuring the absolute total absorption α of a humid air sample signal compared with a dry air reference signal, we measured the relative total absorption $\Delta\alpha_x$ between the sample and reference signals with different humidity levels. The designation of $\Delta\alpha_x$ indicates that there will be a cross term due to the quadratic part of the continuum absorption,

$$\Delta\alpha_x = \alpha^S - \alpha^R = \left(\alpha_{MRT}^S + \alpha_c^S\right) - \left(\alpha_{MRT}^R + \alpha_c^R\right) = \Delta\alpha_{MRT} + \left(\alpha_c^S - \alpha_c^R\right) = \Delta\alpha_{MRT} + \Delta\alpha_{cx}. \quad (9)$$

where the α^S, α_{MRT}^S, α_c^S and α^R, α_{MRT}^R, α_c^R denote the absolute total absorption, the absolute vV-W resonance absorption, and absolute continuum absorption of the sample and reference signals, respectively. The relative resonance line absorption $\Delta\alpha_{MRT}$ is linearly proportional to water vapor number density. Based on Eq. (8), the relative continuum absorption including the cross term $\Delta\alpha_{cx}$ is given by,

$$\Delta\alpha_{cx} = \alpha_c^S - \alpha_c^R = v^2 \left[C_W^* \cdot \left(\left(\rho_W^S\right)^2 - \left(\rho_W^R\right)^2 \right) + C_A^* \cdot \rho_A \cdot \left(\rho_W^S - \rho_W^R\right) \right]. \quad (10)$$

where ρ_W^S and ρ_W^R are water vapor density of the sample and reference signals respectively, and the density difference is $\Delta\rho_W = \rho_W^S - \rho_W^R$. Substituting $\rho_W^S = \rho_W^R + \Delta\rho_W$ in Eq. (10), we obtain:

$$\Delta\alpha_{cx} = v^2 \left[C_W^* \cdot \left(2\rho_W^R \Delta\rho_W + \Delta\rho_W^2\right) + C_A^* \cdot \rho_A \cdot \Delta\rho_W \right]. \quad (11)$$

and the cross term function X is given by

$$X = v^2 C_W^* \left(2\rho_W^R \Delta\rho_W\right). \quad (12)$$

The cross term X has to be subtracted from the relative continuum absorption $\Delta\alpha_{cx}$ and from the relative total absorption $\Delta\alpha_x$. Equations (13a) and (13b) give the absolute continuum absorption $\Delta\alpha_c$ and the absolute total absorption $\Delta\alpha$, which only depend on $\Delta\rho_W$.

$$\Delta\alpha_c = \Delta\alpha_{cx} - X = v^2 \left[C_W^* \cdot \Delta\rho_W^2 + C_A^* \cdot \rho_A \cdot \Delta\rho_W \right]. \quad (13a)$$

$$\Delta\alpha = \Delta\alpha_x - X. \quad (13b)$$

#201718 - $15.00 USD Received 21 Nov 2013; revised 10 Feb 2014; accepted 11 Feb 2014; published 19 Feb 2014

The value of the water vapor density of the reference THz signal ρ_W^R in the additional cross term $\rho_W^R \Delta\rho_W$ can be obtained from the water vapor partial pressure measured by hygrometers in the sample chamber. The quadratic frequency dependence of the continuum absorption was confirmed in our experiments.

In order to determine the cross-term function X and the continuum absorption $\Delta\alpha_c$, we must first determine C_W^* and C_A^*. This is done by using Eq. (11) and two measured values of $\Delta\alpha_{cx}$ for the same window, same reference, but different water vapor densities $\Delta\rho_W$. Inserting the parameters for each measurement into Eq. (11) gives two linearly independent equations, that can be solved for C_W^* and C_A^*. Now, the cross-term function X can be evaluated and then subtracted from $\Delta\alpha_{cx}$ to obtain the continuum absorption $\Delta\alpha_c$.

3. Experimental methods

Figure 2 shows the long-path THz system for the experimental measurement of the continuum absorption described in [20]. The THz pulses are generated and detected by the standard THz TDS system [18], which is coupled to the 170 m round trip long-path THz setup by combining an optical train of large flat mirrors and a spherical telescope mirror [3,4,17,20]. In order to obtain the high signal-to-noise ratio of coherent sampling, the final THz pulses propagation distance of 170.46 m from M1 to M10 was adjusted to be precisely an integer multiple

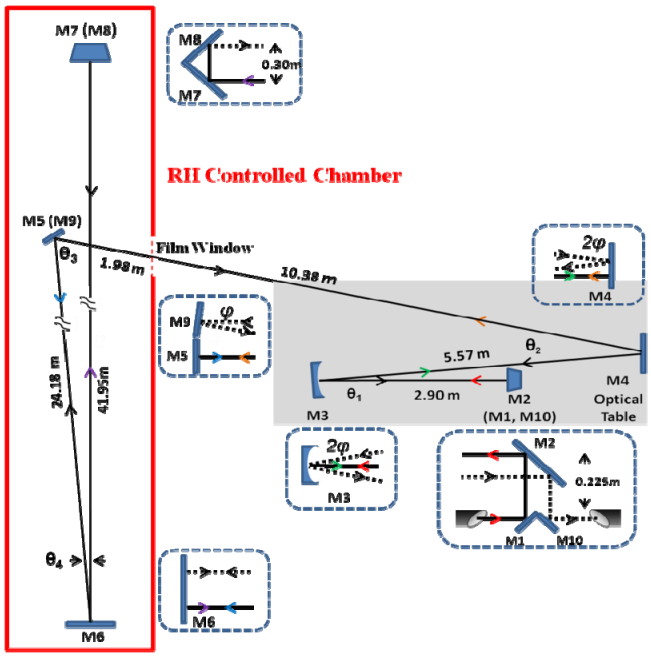

Fig. 2. Experimental set up with 170 m long-path system.

(51 in this case) of the laser pulse round-trip of 3.342 m in the mode-locked laser with a repetition rate of 89.6948 MHz,. A humidity controlled sample chamber, transformed from the THz lab hallway, is shown by the red box in Fig. 3 within the long path. This chamber with 137 m total round trip length (from the entrance through the film window, through the chamber and to the exit through the film window) allowed us to increase the chamber humidity up to RH 30% higher than the ambient laboratory atmosphere. Three hygrometers

#201718 - $15.00 USD Received 21 Nov 2013; revised 10 Feb 2014; accepted 11 Feb 2014; published 19 Feb 2014

measure the RH and temperature during experiments at both ends of the chamber and on the optical table, shown as the gray rectangle in Fig. 2.

The THz long path system with the humidity controlled chamber allowed the relative measurement of the transit time of the sharp leading edge of the reshaped THz pulses propagated through atmosphere to a precision of 0.1 ps, by using the mode-locked laser as an accurate optical clock. The measured THz pulses and their corresponding Fourier-transformed frequency spectra are shown in Fig. 3, for two groups of measurements taken on two different days, 20 days apart. The measured THz pulses in each group were recorded from the same start position of the time scan, which allowed obtaining the transit time difference between the THz pulses with various RH, as shown in Figs. 3(a) and 3(c). The time values in ps at the beginning of the THz signals are the absolute transit time from the start point.

The frequency spectra in Figs. 3(b) and 3(d) are averages of three THz pulses in each set. The frequency independent part of water vapor refractivity is (n-1) = 61.6 x 10^{-6} in an atmosphere with RH 58% at 20 °C (density of 10 g/m^3) [23]. The transit time of THz pulses through the 137 m total round-trip path in the RH (density 10 g/m^3) controlled chamber is 27.9 ps longer, than for a dry chamber. By comparing the transmitted time difference Δt of the sample and reference pulses with 27.9 ps / 10 g/m^3, the relative water vapor density can be calculated to an accuracy of 0.04 g/m^3, corresponding to RH 2%, and a 0.1 ps delay change.

In this work, the transit times of THz pulses are not only affected by various RH levels but also by the laser-clock drift and the drift in the long THz optical train. Firstly, the repetition (clock) rate of the Mode-locked laser is 89.6948xx MHz, measured to eight digits by a frequency counter, is quite stable to six digits during measurements. Frequency drift and some jitter occur in the last 2 digits as indicated by xx which illustrates a slow change in the optical clock rate of the order of 100 Hz.

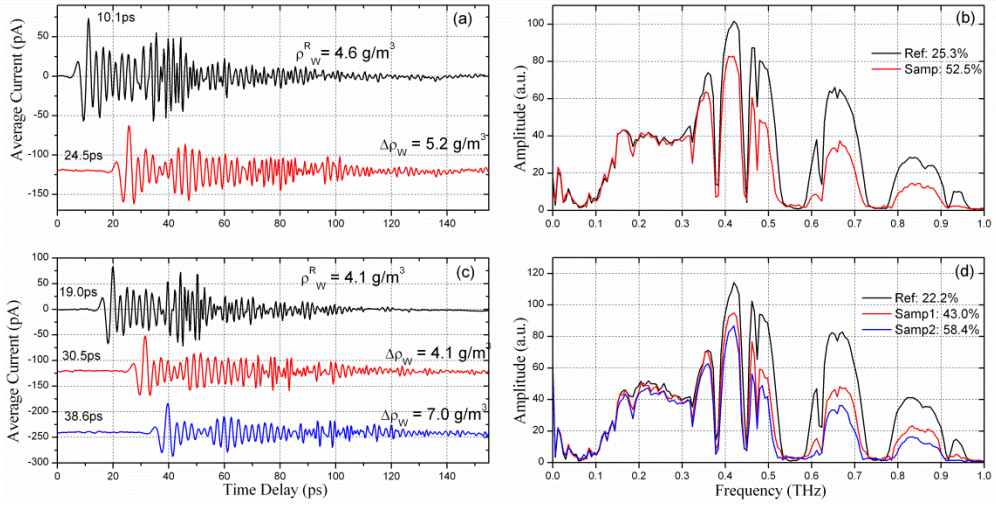

Fig. 3. The measured transmitted THz pulses and the corresponding amplitude frequency spectra for humidity levels on different days. (a) Reference pulse (top trace) and sample pulse (bottom trace). (b) Amplitude spectra corresponding to (a). (c) Reference pulse (top trace) and two sample pulses (lower traces). (d) Amplitude spectra corresponding to (c).

Secondly, the slow change of the length of the long THz optical train is from the heat expansion and cold contraction of the concrete floor and stainless steel (SS) optical table [20]. The massive concrete floor has very slow response to average temperature changes, on the order of many hours or days, while the temperature response of the SS table is much faster. Moreover, stainless steel and concrete have approximately the same coefficient of thermal

#201718 - $15.00 USD Received 21 Nov 2013; revised 10 Feb 2014; accepted 11 Feb 2014; published 19 Feb 2014

expansion 10^{-5} (ΔL/L)/°C. If the difference temperature ΔT changed by 1 °C, a length difference of 170 m x 10^{-5} would occur, with the corresponding change in the start time of the THz pulse of 5.7 ps. This time change is approximately equal to the observed day to day and week to week changes as shown in the difference groups of THz signals in Fig. 3.

From the experimental results, the stable transit times for several scans in a series show the stability of the long-path setup and that no significant change in optical train or laser-clock drift occurs. The weak water vapor absorption line center frequencies in the Fourier-transformed frequency spectra of measurements shown in Fig. 2 agree with the HITRAN and the JPL database to an accuracy of 1 GHz [17], which indicates the stability of the long-path setup within one scan.

4. Results

The relative amplitude transmission of sample #2 with respect to the reference of Fig. 3(d) is shown in Fig. 4(a) for the path length of 137 m. This transmission was obtained by dividing the sample amplitude spectrum by the reference spectrum as shown in Fig. 3(d). The corresponding absorption $\Delta\alpha_x$ shown in Figs. 4(b) and 5(a) were obtained by taking the log to the base 10 of the values of transmission per km, multiplied by 20 to obtain the power absorption.

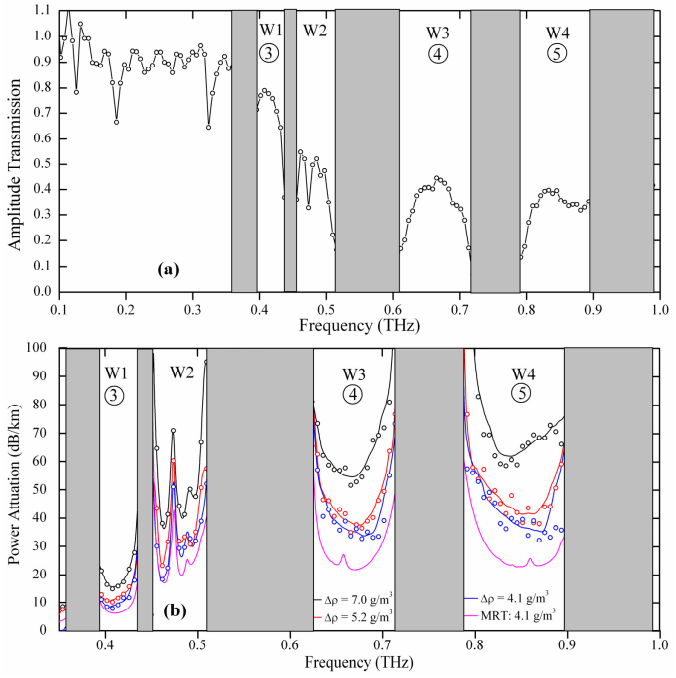

Fig. 4. (a) Amplitude transmission for $\Delta\rho_w$ = 7.0 g/m^3, which is the spectral ratio between the sample #2 and reference in Fig. 3(d). (b) Measured power attenuation coefficients $\Delta\alpha_x$ (open circles) in dB/km with the smoothed THz windows W1-W4 (solid lines), for the water vapor density differences of $\Delta\rho_w$ = 4.1 g/m^3 (bottom blue circles), $\Delta\rho_w$ = 5.2 g/m^3 (middle red circles) and $\Delta\rho_w$ = 7.0 g/m^3 (top black circles). For comparison the MRT calculation for $\Delta\rho_w$ = 4.1 g/m^3 is shown as the purple solid bottom line. ③-⑤ indicate the THz windows investigated in [19].

In Fig. 4, four THz transmission windows at 0.41 THz (W1), 0.46 – 0.49 THz (W2), 0.68 THz (W3) and 0.85 THz (W4) are shown clearly within 0.35 – 1 THz. The grey regions

#201718 - $15.00 USD Received 21 Nov 2013; revised 10 Feb 2014; accepted 11 Feb 2014; published 19 Feb 2014

cover the no-signal areas, caused by the strong water vapor absorption lines. In Fig. 4(b), in order to minimize the ripple effect, the smoothed measured window curves were obtained by using the Matlab smooth command for 5 points in W1 and W3, 8 points in W4, and none for W2. The ripples on the measurements are caused by small reflections following the main pulse, from surfaces other than the coupled mirrors.

The measured relative total absorption $\Delta\alpha_x$ and the calculated relative resonance absorption for the water vapor density difference of $\Delta\rho_W$ = 7.0 g/m^3 are shown in Fig. 5(a). The difference between the measured smoothed windows $\Delta\alpha_x$ (red solid line) and the calculated relative resonance absorption (black solid line) is the relative continuum absorption $\Delta\alpha_{cx}$ described by Eq. (10), which includes the cross term *X*. Analysis of the measurements of $\Delta\alpha_{cx}$ in Fig. 5(a), allowed us to determine the corresponding *X*, shown as the lowest dashed curve. X is shown for all three measurements in Fig. 5(b). We determined the values of relative continuum absorption $\Delta\alpha_{cx}$ and *X* at each window, from the difference between the minima of the calculated resonance absorption windows to the minimum of the smoothed windows as shown in the bottom of Fig. 5(a).

The differences $\Delta\alpha_{cx}$ between minima of the measurement and the $\Delta\rho_W$ = 7.0 g/m^3 MRT curve for each window shown in Fig. 5(a) are presented in Table 1, together with the corresponding cross-term *X* and the desired absolute continuum absorption $\Delta\alpha_c$. These same parameters are listed in the table for $\Delta\rho_W$ = 4.1 g/m^3 and $\Delta\rho_W$ = 5.2 g/m^3. Figures 5(b) and 5(c) show the corresponding values taken from the table, showing excellent agreement with the squared frequency dependence of Eqs. (7)–(13). The theoretical curves presented in Figs. 5(b) and 5(c) are obtained from Eqs. (12) and (13a) with $C_W^* = (1.33)^2 C_W$ and $C_A^* = (1.33\times 0.84)C_A$, where C_W and C_A are given in Table 2.

In Fig. 5(c), the dashed lines for the three curves show that part of the continuum absorption due to the linear dependence on $\Delta\rho_W$, the difference between the two curves shows that part of the absorption due to the $\Delta\rho_W^2$ quadratic components. It is noteworthy that the fraction shows this $\Delta\rho_W^2$ dependence, but it is somewhat surprising that the quadratic term $\Delta\rho_W^2$ is such a relatively small fraction of the total. For example, for 7.0 g/m^3 the quadratic term is 33% of the total, and for 5.2 g/m^3 the term (highlighted in yellow) is 25% and for 4.1 g/m^3 the term is 20%.

In Fig. 5(c), it is informative to compare the ratio of the MRT resonant line absorption to the empirically fit continuum absorption, $R_\alpha = \alpha_{MRT}/\alpha_{c,}$ for the THz windows of transparency: for W4 at 850 GHz, R = 2.5, For W3 at 680 GHz, R = 3.3, for W2 at 475 GHz, R_α = 6.0, for W1 at 410 GHz R_α = 2.7, for the window at 345 GHz, R_α = 1.7, for the window at 220 GHz, R_α = 0.74, and at 100 GHz, R_α = 0.33. For the windows below 300 GHz, the continuum absorption has become larger than the MRT absorption. This situation has driven much interest in mm wave applications, for which the continuum absorption is the major component.

Our empirical curve of Fig. 5(c), and the associated MRT resonant line absorption are in acceptable agreement with the recent simulation of the two optimal THz communication links in the atmosphere at 95 GHz, and 250 GHz [24]. In that work for 10 g/m^3 at 20 °C, at 95 GHz, α_c = 0.25 dB/km, and $\alpha_{vV\text{-}W}$ = 0.27 dB/km, total α = 0.52 dB/km; at 250 GHz, α_c = 2.8 dB/km, and $\alpha_{vV\text{-}W}$ = 1.5 dB/km, total α = 4.3 dB/km. These values are comparable to our values shown in Fig. 5(c) (increased by 10/7 to account for the different water vapor density). Our increased values are for 100 GHz, α_c = 0.34 dB/km, and α_{MRT} = 0.21 dB/km, total α = 0.55 dB/km; For 250 GHz, α_c = 2.1 dB/km, and α_{MRT} = 1.43 dB/km, total α = 3.53 dB/km.

#201718 - $15.00 USD Received 21 Nov 2013; revised 10 Feb 2014; accepted 11 Feb 2014; published 19 Feb 2014

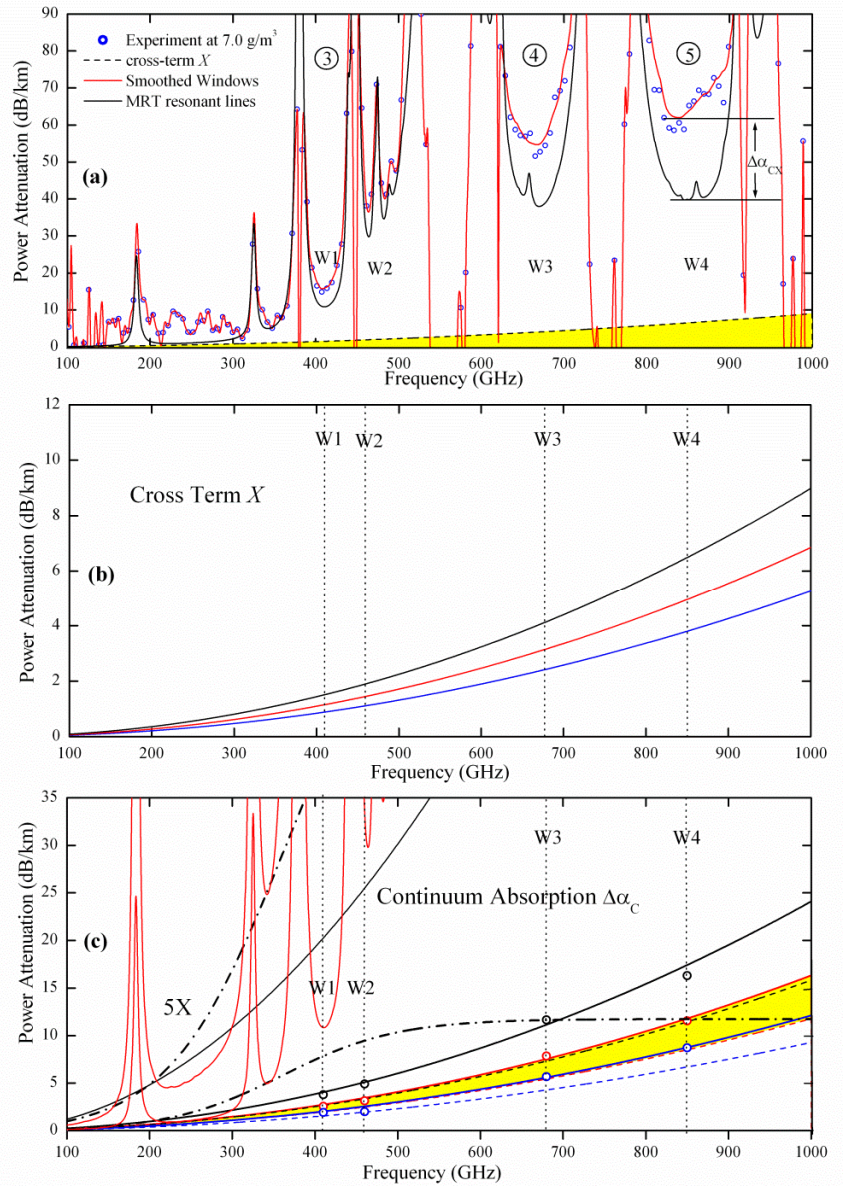

Fig. 5. (a) Illustration of the method to obtain the relative continuum absorption $\Delta\alpha_{cx}$ for the windows with $\Delta\rho_w$ = 7.0 g/m^3. The measured total absorption (blue circles), smoothed measured THz window (red solid line), the resonance absorption with MRT lineshape (black line). The quadratic fitting for X (black dash line) with yellow highlight for $\Delta\rho_w$ = 7.0 g/m^3. (b) The calculated cross term X absorption with a quadratic frequency dependence, $\Delta\rho_w$ = 7.0 g/m^3 (top black line), $\Delta\rho_w$ = 5.2 g/m^3 (middle red line), and $\Delta\rho_w$ = 4.1 g/m^3 (bottom blue line). (c) The continuum absorption $\Delta\alpha_c$ from Table 1 and corresponding fitting (solid lines), the linear $\Delta\rho_w$ component (dash lines), and the historical curve in [24,25] for 7 g/m^3 (dash dot line). The MRT calculation of Fig. 5(a) is shown as the lower red curve and is also shown as the 5X magnified red curve. The comparison between the empirical theory and historical curve below 400 GHz are also shown with a 5X magnification.

#201718 - $15.00 USD Received 21 Nov 2013; revised 10 Feb 2014; accepted 11 Feb 2014; published 19 Feb 2014

The self and foreign broadened parameters, which have been obtained from different studies [9,12,13] and this work are shown in Table 2. Our pressure-related continuum parameters C_W and C_A do not agree with those of [12,13], as expected, since they used the vV-Wc model and the linear prefactor for the vV-W lineshape function. Moreover, our ratio of C_W/C_A = 56.2, for the contribution of dimers to that of the water-air collisions comprising the total continuum absorption, as described in Eq. (13a), is much higher than that for the other two THz measurements of 18.6 in [12] and 10.9 in [13]; and is significantly higher than that for the millimeter measurement of 30.2 in [9].

We present our measurement of $\Delta\alpha$ and the absorption of the transparent THz windows for our conditions in Fig. 6. This figure was obtained from Fig. 5(a) by subtracting X from the measurements of $\Delta\alpha_x$ as described in Eq. (13b). We can compare these results to those in Table 1 of [19], by adjusting our measurements at 7.0 g/m^3 to 9.3 g/m^3, corresponding to multiplying the measurements in Fig. 6, by 1.33. We then obtain the minimum absorptions in our windows ③, ④, and ⑤ of 19 dB, 68 dB, and 72 dB respectively to be compared with the previous measurements in windows ③, ④, and ⑤ of 28 dB, 72 dB and 92 dB, respectively [19]. We consider the work presented here to be more precise because of the extra path length. We note the quite good agreement with historic Fig. 1* explained in [25], which has the values of 22.9 dB, 70.5 dB and 75.1 dB respectively.

Table 1. Determined Values of $\Delta\alpha_{cx}$, X, $\Delta\alpha_c$ in dB/km at Four THz Windows with Different Density

Windows	$\Delta\rho_w$(4.1 g/m^3)			$\Delta\rho_w$(5.2 g/m^3)			$\Delta\rho_w$(7.0 g/m^3)		
All values (dB/km)	$\Delta\alpha_{cx}$	X	$\Delta\alpha_c$	$\Delta\alpha_{cx}$	X	$\Delta\alpha_c$	$\Delta\alpha_{cx}$	X	$\Delta\alpha_c$
W1	2.8	0.9	1.9	3.7	1.2	2.5	5.3	1.5	3.8
W2	3.1	1.1	2.0	4.2	1.4	2.8	6.8	1.9	4.9
W3	8.1	2.4	5.7	11.0	3.2	7.8	15.8	4.2	11.6
W4	12.5	3.8	8.7	16.5	4.9	11.6	22.5	6.5	16.0

Table 2. Laboratory Determinations of Water Vapor Self and Foreign Continuum Parameters in Millimeter Wave and THz Range. C_W and C_A Parameters Are in Units of dB/km/(GHz hPa)^2

Reference	C_W (x10^{-7})	C_A (x10^{-9})	n_s	n_f	Experimental conditions	Database	v-VW Pre-factor	Cutoff (GHz)
This Work	0.95	1.69	NA	NA	0.35-1 THz 294 K	HITRAN	$(\nu/\nu_j)^2$	None
Slocum [13]	0.45	4.12	NA	NA	0.3-1.5 THz 296 K	HITRAN	ν/ν_j	None
Podobedov [12]	0.48*	2.55*	5.50	1.80	0.3-2.7 THz 293-333 K	HITRAN	ν/ν_j	750
Koshelev [9]	0.94*	3.11*	5.24	0.91	107-143 GHz 261-328 K	R98 [14]	$(\nu/\nu_j)^2$	750

*The values are calculated from original C^0_W for 294 K.

5. Conclusions

This study experimentally and theoretically investigates the important, but poorly understood water vapor continuum absorption within the 0.35 – 1 THz range, using the long path THz-TDS system. We demonstrated that accurate average relative humidity (RH) changes for the THz path can be obtained by measuring the humidity-dependent different transit times to an

#201718 - $15.00 USD Received 21 Nov 2013; revised 10 Feb 2014; accepted 11 Feb 2014; published 19 Feb 2014

accuracy of 0.1 ps of the THz pulses, that have propagated through the 137 m round-trip path within the humidity controlled sample chamber.

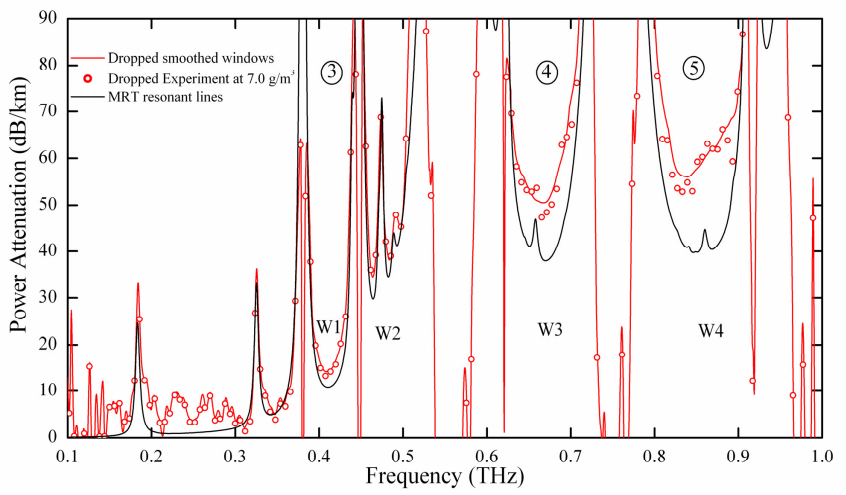

Fig. 6. The measured absolute total absorption $\Delta\alpha$ (red dots) and the resonance absorption with MRT lineshape (black line) for $\Delta\rho_w$ = 7.0 g/m^3.

Because the continuum absorption α_c is defined as the difference between the measured total absorption and the resonant line absorption, it is very important that the resonant absorption has a strictly defined lineshape function to obtain reliable results. Previous work has used linear (v/v_j) or quadratic $(v/v_j)^2$ pre-factors with the van Vleck Weisskopf (vV-W) lineshape function, which leads to differences in the evaluated continuum absorption. We showed that the quadratic pre-factor should be used with the vV-W lineshape, and with the JPL and HITRAN databases.

We used Molecular Response Time theory (MRT), which has no cut-off, to obtain the resonant line absorption. As shown in Fig. 1, the MRT lineshape consists of a frequency dependent fractional sum of the vV-W absorption and the full Lorentz (FL) absorption, for which the weighting factor is determined by the frequency and the molecular response time τ_c. Consequently, the MRT resonant absorption is always between the vV-W and FL values of absorption. These fundamental limits showed that the abrupt 750 GHz cut-off shown in Fig. 1, related to an approximate collision duration of 1 ps, is too severe in reducing the resonant absorption and thereby increasing the continuum absorption. In contrast, as shown in Fig. 1, the MRT lineshape smoothly changes from vV-w to FL as the frequency increases. The rate of this transition is determined by the molecular response time τ_c, which has been measured for the methyl halides to be τ_c = 0.2 ps [21,22]. This approach allowed us to make definitive measurements of the smaller continuum absorption under our conditions.

Our continuum absorption determinations in the four water vapor,THz windows of transparency at 0.41 THz, 0.46 THz, 0.68 THz and 0.85 THz, showed humidity-dependent changes in a good agreement with the empirical continuum theory. Using these results with the empirical theory, the predicted continuum absorption α_c for much lower frequencies is larger than the resonant line absorption, consistent with previous mm-wave determinations.

We plan future continuum determinations with higher precision, obtained by a much reduced RH of the reference pulse and an increase in the holding time of the sample chamber. Lower reference RH would be possible on a cold dry day in winter, for which the ambient humidity in the laboratory can be less than RH 10%, corresponding to ρ_w = 1.7 g/m^3. A longer holding time in the chamber would allow larger increases in the contained RH. We also plan to increase the spectral amplitudes of the lower frequencies from 95 GHz to 350 GHz, by

#201718 - $15.00 USD Received 21 Nov 2013; revised 10 Feb 2014; accepted 11 Feb 2014; published 19 Feb 2014

using different THz transmitters and receivers and larger long-path mirrors, to enable us to measure the important water vapor, THz windows in this range, for which $\alpha_{MRT} < \alpha_c$.

Appendix A: Pre-factor of vV-W lineshape

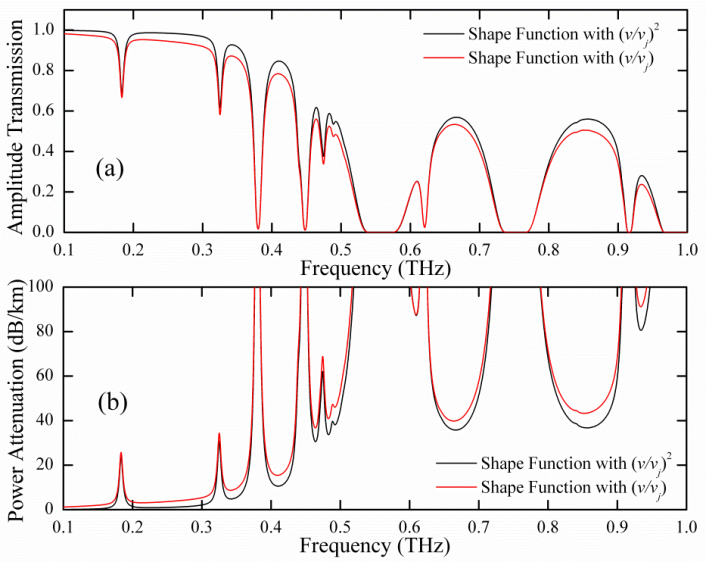

Fig. 7. (a) The calculated amplitude transmissions of the two different pre-factor vV-W lineshapes after 137 m propagation at RH 37% and 20 °C which is equivalent to density of 6.4 g/m^3, using the quadratic term of Eq. (2) (upper black line) and using the linear term of Eq. (3) (lower red line). (b) Corresponding power attenuation in dB/km.

The calculated resonance amplitude transmissions after 137 m propagation with water vapor density of 6.4 g/m^3 based on two types of v-VW lines shapes are shown in Fig. 7. The linear pre-factor curve using Eq. (3) shows a significantly lower transmission than the quadratic pre-factor curve using Eq. (2) from 0 to 1 THz. Consequently, the continuum absorption obtained by the linear v/v_j pre-factor would be smaller than that obtained by the quadratic $(v/v_j)^2$ pre-factor.

The quadratic pre-factor vV-W lineshape function will now be shown to be required for the JPL database, based on the direct conversion of the absorption expression in the original vV-W paper [15] from the classic oscillator to quantum mechanics below 2 THz. In the JPL database the absorption coefficient $\alpha_j(v)$ of water vapor resonant line can be written as the product of a line intensity I_j with units of (nm^2 MHz) and a lineshape function $f(v, v_j)$ [4,7]: where N_{H2O} is the number density of water vapor in molecules / (cm·nm^2), and v_j is the water vapor resonant line center frequency in MHz.

$$\alpha_j(v) = N_{H2O} \cdot I_j(v) \cdot f(v, v_j). \tag{14}$$

where N_{H2O} is the number density of water vapor in molecules / (cm·nm^2), and v_j is the water vapor resonant line center frequency in MHz.

The absorption coefficient equation in the HITRAN database has the same format as $\alpha_j(\tilde{v}) = N^*_{H_2O} \cdot S_j(\tilde{v}) \cdot f(\tilde{v}, \tilde{v}_j)$, where $N^*_{H_2O}$ is the number density of water vapor in molecules / (cm^3), S_j is the intensity in a cm^{-1}/(molecule/cm^2) and $\tilde{v}_j$ is the water vapor resonant line center wavenumber in cm^{-1}. Note that S_j can be converted to I_j by $S_j = I_j / (c \cdot 10^{10})$ where c is the speed of light in vacuum with units of m/s [6]. For both the

#201718 - $15.00 USD Received 21 Nov 2013; revised 10 Feb 2014; accepted 11 Feb 2014; published 19 Feb 2014

JPL and the HITRAN databases, the total absorption coefficient is the sum of all of individual water vapor absorption lines by using the line-by-line summation method as $\alpha = \sum_j \alpha_j$.

The original vV-W paper [15] shows how the vV-W lineshape functions can be used with the JPL database. Firstly, the classical oscillator theory expression of absorption per unit length is given by Eq. (17) in [15] and Eq. (13-16) in [16]:

$$\alpha = \frac{Ne^2}{mc}\left(\frac{v}{v_0}\right)^2\left[\frac{1/2\pi\tau}{\left(v-v_0\right)^2+\left(1/2\pi\tau\right)^2}+\frac{1/2\pi\tau}{\left(v+v_0\right)^2+\left(1/2\pi\tau\right)^2}\right]. \tag{15}$$

where τ is the mean time interval between collisions and $1/\tau = 2\pi\Delta v$. In order to convert the classic oscillator expression to the general quantum-mechanical system, the factor e^2/m was replaced by $8\pi^2 v_j \left|\mu_{ba}^2\right|/3h$, (*b* and *a* in this quantum-mechanical expression denote the excited and lower states respectively, of the transition v_j), where μ_{ab} is the corresponding dipole moment matrix element [15,16,26]. Following Eqs. (13-17) through 13-19 in [16], we have replaced N with Δn_j , which is the number density difference between the lower and excited states of transition v_j.

$$\alpha_j = \Delta n_j \frac{8\pi^2 v_j \left|\mu_{ba}\right|^2}{3hc}\left(\frac{v}{v_j}\right)^2\left[\frac{1/2\pi\tau}{\left(v-v_j\right)^2+\left(1/2\pi\tau\right)^2}+\frac{1/2\pi\tau}{\left(v+v_j\right)^2+\left(1/2\pi\tau\right)^2}\right]. \tag{16}$$

The number density n_j in the lower state of the v_j transition is given by

$$n_j = Nf_{ja}. \tag{17}$$

where N is the total number density and f_{ja} is the fractional factor [16],

$$f_{ja} = \left(2J+1\right)e^{-E_{ja}/kT}\Big/\sum_{j,J}\left(2J+1\right)e^{-E_{ja}/kT}. \tag{18}$$

The number density difference Δn_j is given by

$$\Delta n_j = n_j\left(1-e^{-\left(E_{jb}-E_{ja}\right)/kT}\right). \tag{19}$$

where $E_{jb}-E_{ja}=hv_j$, and for $hv_j \ll kT$ is well approximated by $\Delta n_j \approx n_j\left(hv_j/kT\right)$. Substituting these results in Eq. (15), we obtain

$$\alpha_j = N\left[\frac{8\pi^3}{3ckT}\cdot\frac{v_j^2\left|\mu_{ba}\right|^2\left(2J+1\right)e^{-E_{ja}/kT}}{\sum_{j,J}\left(2J+1\right)e^{-E_{ja}/kT}}\right]\cdot\frac{1}{\pi}\left(\frac{v}{v_j}\right)^2\left[\frac{1/2\pi\tau}{\left(v-v_j\right)^2+\left(1/2\pi\tau\right)^2}+\frac{1/2\pi\tau}{\left(v+v_j\right)^2+\left(1/2\pi\tau\right)^2}\right]. \tag{20}$$

which is in exact agreement with Eq. (13-19) in [16]. Now the absorption coefficient α_j shown in Eq. (20) is seen to be a product of the total number density *N*, the line intensity I_j (in the first bracket) and lineshape function *f(v, v_j)*.

We will now show that I_j in Eq. (20) is identical to the line intensity I_j shown as Eq. (1) in the JPL database [7] which is given below:

$$I_{ba}\left(T\right) = \left(\frac{8\pi^3}{3hc}\right)\cdot\frac{v_{ba}\,{}^{x}S_{ba}\mu_x^2\left[e^{-E_{ja}/kT}-e^{-E_{jb}/kT}\right]}{Q_{rs}}. \tag{21}$$

for $v_{ba}=v_j$, ${}^{x}S_{ba}\mu_x^2 = \left(2J+1\right)\mu_{ab}^2$ according to Eq. (4-28) in [16], and the rotational-spin partition function $Q_{rs}=\sum_{j,J}(2J+1)e^{-E_{ja}/kT}$. Using these relationships and the approximation: $1-e^{-\left(E_{jb}-E_{ja}\right)/kT} \approx hv_j/kT$, for $hv_j \ll kT$, we can rewrite Eq. (21) as

#201718 - $15.00 USD Received 21 Nov 2013; revised 10 Feb 2014; accepted 11 Feb 2014; published 19 Feb 2014

$$I_j = \left(\frac{8\pi^3}{3ckT}\right)\cdot\frac{v_j^2\left|\mu_{ba}\right|^2(2J+1)e^{-E_{ja}/kT}}{\sum_{j,J}(2J+1)e^{-E_{ja}/kT}}. \qquad (22)$$

which is identical to the line intensity I_j in the first brackets of Eq. (20). And the lineshape function $f(v, v_j)$ of Eq. (20) has the quadratic $(v/v_j)^2$ pre-factor which is same as the $f_1(v, v_j)$ of Eq. (2). This quantum-mechanical relationship only holds in the region for $hv_j \ll kT$, which is equivalent to the frequency is much smaller than 6.2 THz, for 300 K [16]. Consequently, the above result for the conversion from classic oscillator to quantum-mechanics is valid below 2 THz and shows that the quadratic pre-factor vV-W lineshape function should be used with the JPL database.

Appendix B: vV-W$_c$ cut-off lineshape

The modified vV-W$_c$ lineshape function with the cut-off [9,11,14], is given by

$$f_{cutoff}\left(v,v_j\right) = \frac{1}{\pi}\left(\frac{v}{v_j}\right)^2\cdot\left(\frac{\Delta v_j}{\left(v-v_j\right)^2+\Delta v_j^2}+\frac{\Delta v_j}{\left(v+v_j\right)^2+\Delta v_j^2}-\frac{2\Delta v_j}{v_{cut}^{\ 2}+\Delta v_j^2}\right). \quad if\ \left|v-v_j\right| < v_{cut} \qquad (23)$$

$$f_{cutoff}\left(v,v_j\right) = 0. \quad if\ \left|v-v_j\right| \geq v_{cut}$$

where v_{cut} is the cutoff frequency of 750 GHz in this work. Using the cutoff increases the calculated transmission of water vapor. However, as pointed out by our referee, Eq. (23) has a physical inconsistency, whereby the calculated value becomes negative for frequency differences from resonance, slightly smaller than the cutoff frequency. Consequently, we developed the straight-forward procedures given in Eqs. (24), (25) and (2) to handle the cutoff and to eliminate this inconsistency. For case 1, of Eq. (23) with $v_j < v$, we have

$$f_{cutoff}\left(v,v_j\right) = \frac{1}{\pi}\left(\frac{v}{v_j}\right)^2\cdot\left(\frac{\Delta v_j}{\left(v-v_j\right)^2+\Delta v_j^2}+\frac{\Delta v_j}{\left(v+v_j\right)^2+\Delta v_j^2}-\frac{\Delta v_j}{v_{cut}^{\ 2}+\Delta v_j^2}-\frac{\Delta v_j}{\left(2v_j+v_{cut}\right)^2+\Delta v_j^2}\right). \qquad (24)$$

for which $f_{cutoff}\left(v,v_j\right) = 0.$, when $v_{cut} \leq (v-v_j)$ For case 2, with $v < v_j$, we have

$$f_{cutoff}\left(v,v_j\right) = \frac{1}{\pi}\left(\frac{v}{v_j}\right)^2\cdot\left(\frac{\Delta v_j}{\left(v-v_j\right)^2+\Delta v_j^2}+\frac{\Delta v_j}{\left(v+v_j\right)^2+\Delta v_j^2}-\frac{\Delta v_j}{v_{cut}^{\ 2}+\Delta v_j^2}-\frac{1}{\left(2v_j-v_{cut}\right)^2+\Delta v_j^2}\right) \qquad (25)$$

for which $f_{cutoff}\left(v,v_j\right) = 0.$, when $v_{cut} \leq (v_j - v)$ For case 3, with $v < v_j < v_{cut}$, we have $f_{cutoff}\left(v,v_j\right) = f_1\left(v,v_j\right)$, given by Eq. (2).

Acknowledgment

This work was partially supported by the National Science Foundation.